Offshore Wind Turbine Loads and Motions in Unstable Atmospheric Conditions

IOP Conf. Series: Journal of Physics: Conf. Series **1356** (2019) 012016 doi:10.1088/1742-6596/1356/1/012016

Offshore Wind Turbine Loads and Motions in Unstable Atmospheric Conditions

R M Putri[1], C Obhrai[1] and J M Knight[1]

[1]Department of Mechanical and Structural Engineering and Material Science, University of Stavanger, Norway

Abstract. Even though it is widely known that unstable atmospheric stability conditions can lead to higher turbulence, the use of proper turbulent wind models considering unstable conditions are not often used in the simulation of loads and motions of offshore wind turbines. For this reason, the Højstrup model, which was specifically developed for unstable conditions, is used to simulate a spar-buoy offshore wind turbine (OWT) and investigate the importance of unstable conditions in the design of floating offshore wind turbines. It is found that fatigue damage of a spar-buoy OWT is strongly influenced by unstable conditions, where very unstable condition gives 65% higher fatigue damage than neutral conditions for the tower top torsion, followed by 37% higher for tower base side-side bending and 24% higher for blade root flap-wise mode.

1. Introduction

The fast development of offshore wind turbines in the recent years has brought offshore wind into deeper waters with the help of floating platform concepts. Floating platform concepts can be divided in three different groups based on how the platform gains stability: buoyancy, station-keeping system, and gravity-based. The buoyancy group relies on the water plane area to gain its stability, such as a barge type floater. Tensioned-leg platform falls into the station-keeping system group where it depends on its tendons both to gain stability and as a station-keeping system. The gravity-based group relies on its weight to gain stability where spar-floater is included in this group since the platform is ballasted to obtain sufficient weight. While the knowledge of floating platforms is available from the oil and gas experience, the use of large rotor turbines on floating platforms has become a challenge due to uncertainties in turbulent wind models which may cause excessive platform motions. Depending on the floater type, a specific degree of freedom (DOF) could be more prominent than other DOFs. Excessive motions can also lead to severe fatigue damage on floating offshore wind turbine (FOWT) components which need to be thoroughly assessed in the design of FOWTs.

One of the reasons for the pronounced platform motions is the excitation from low frequency turbulent wind that is within the range of floating platforms natural frequencies (< 0.05 Hz for typical platform translation DOFs). When considering turbulent wind, the influence of air temperature –known as atmospheric stability– cannot be ignored except for the case of extreme winds [1]. Atmospheric stability is associated with vertical movement of air parcels depending on air's temperature. When the air parcels' temperature is colder than the surrounding air, then they sink resulting in stable conditions. The opposite creates unstable conditions where air parcels are warmer than the surrounding air and they rise creating buoyant-generated turbulence. By including the effect of atmospheric stability, a more accurate fatigue load and platform motion estimation can be achieved for the design of FOWTs. In the current available OWT design standard (IEC 61400 [2]) two turbulent wind models are recommended by assuming only neutral atmospheric conditions: the Kaimal model with a given exponential coherence model and the Mann uniform shear turbulence model [3]. Meanwhile, analysis of offshore wind

measurement data has shown that unstable atmospheric conditions are most prevalent offshore, notably during winter time composing approximately 48.6% occurrence in a year [4].

This study aims to investigate the influence of unstable atmospheric conditions on the OC3-Hywind turbine [5] loads and motions with the use of the Højstrup 1981 [6] wind model. These results were compared with the Kaimal model [7] which represents neutral atmospheric conditions. MATLAB codes [8] were used to generate turbulent wind fields based on the Højstrup spectral model combined with the Davenport Coherence function [9], as well as the Kaimal spectral model combined with the Davenport Coherence function as input to coupled SIMO-RIFLEX [10] simulations of the OC3-Hywind.

2. Theoretical background

Højstrup spectral model is one of the turbulent wind models designed to simulate unstable atmospheric conditions. The model was developed based on measurements taken in Kansas in 1968 and Minnesota in 1973, and showed a good agreement with data from the RISØ 1978 experiment [6]. This model is an extension of the Kaimal spectral model and comprises two semi-empirical spectra [6]:

$$S(n) = S_L(n) + S_M(n) \tag{1}$$

where $S_M(n)$ is the Kaimal spectra and $S_L(n)$ characterises the low-frequency part of the spectra [6]. The low frequency part of the spectra may be important when considering the loads and motions of large FOWTs as their natural frequencies tend to lie within the low frequency range.

Kaimal spectra are derived based on the Kansas measurements with the approach of collapsing all spectra into universal curves in the inertial subrange, and the spectral behaviour at lower frequencies are observed as a function of the stability parameter z/L (where z is height above surface and L is Obukhov length) [7]. Inertial subrange spectral behaviour converges to a -2/3 line at the high frequency end, while at low frequencies, the spectra depend on z/L [7]. The empirical spectral formulas for neutral lapse rate as proposed by Kaimal for u, v, and w wind components are [7]:

$$\frac{nS_u(n)}{u_*^2} = \frac{105\,f}{(1+33\,f)^{5/3}} \tag{2}$$

$$\frac{nS_v(n)}{u_*^2} = \frac{17\,f}{(1+9.5\,f)^{5/3}} \tag{3}$$

$$\frac{nS_w(n)}{u_*^2} = \frac{2\,f}{1+5.3\,f^{5/3}} \tag{4}$$

where u_* is the friction velocity, f is the dimensionless frequency (nz/U), U is the mean horizontal wind velocity and n is frequency. The above spectra represent $S_M(n)$ component in the Højstrup model and the addition of low frequency part $S_L(n)$ will complete the Højstrup spectral equations. The Højstrup model can then be written as [6]:

$$\frac{nS_u(n)}{u_*^2} = \frac{0.5\,f_i}{1+2.2\,f_i^{5/3}}\left(\frac{z_i}{-L}\right)^{2/3} + \frac{105\,f}{(1+33\,f)^{5/3}} \tag{5}$$

$$\frac{nS_v(n)}{u_*^2} = \frac{0.32\,f_i}{1+1.1\,f_i^{5/3}}\left(\frac{z_i}{-L}\right)^{2/3} + \frac{17\,f}{(1+9.5\,f)^{5/3}} \tag{6}$$

$$\frac{nS_w(n)}{u_*^2} = \frac{32\,f}{(1+17\,f)^{5/3}}\left(\frac{z}{-L}\right)^{2/3} + \frac{2\,f}{1+5.3\,f^{5/3}} \tag{7}$$

where $f_i = nz_i/U$ and z_i is the lowest inversion height. S_w in Equation (7) is expressed in terms of f and not f_i since the velocity fluctuations of the w-component is limited by the presence of the solid surface, hence it does not scale with z_i and f_i [6]. When parameter L approaches infinity, then Equation (5) to (7) are reduced to the Kaimal spectra in (2) to (4), describing neutral atmospheric conditions. In this study, the u_* value is approximated with u_{*0} according to Højstrup [11] and formulated as:

$$u_* = u_{*0}\left(1 - \frac{z}{z_i}\right) \tag{8}$$

As can be seen from (5) to (7), parameters affecting the Højstrup model include z, z_i, L, and u_*. Since height (z) is a physical measure and not a representative of meteorological condition, we will neglect the presence of z. Instead, we refer to a stability parameter z/L which indirectly represents parameter L. The lowest inversion height z_i represents the height of the boundary layer, which is influenced by atmospheric stability conditions. From stable to unstable conditions, z_i increases as shown in [4], where they found from measurements at an offshore site (FINO1) that z_i varies from approximately 700 m for unstable, 431 m for neutral, and drops to 104 m for stable conditions. Likewise, Obukhov length L represents the effect of shear friction to buoyancy ratio towards the vertical air movement and characterises the turbulence in the surface layer [12]. The sign of L depends on the temperature gradient. In the case of stable conditions, the temperature gradient is positive and results in positive L. The opposite is true for unstable conditions where the temperature gradient is negative.

Table 1. Parametric study of the Højstrup model

z_i (m)	L (m)	TI_u (%) at z = 90 m	TI_u (%) at z = 167.5 m
		1.02	1.00
		3.05	3.01
		6.10	6.01
1000	-100	**8.13**	**8.02**
		12.20	12.02
		18.30	18.03
		24.40	24.05
300		5.56	5.46
500		6.30	6.19
700		6.80	6.69
900	-100	7.73	7.61
1000		**8.13**	**8.02**
1500		8.85	8.73
2000		9.35	9.23
	-1500	6.69	6.50
	-1000	6.78	6.58
	-700	6.89	6.68
1000	-400	7.12	6.91
	-100	**8.13**	**8.02**
	-50	9.01	8.97
	∞	6.36	6.15

To understand the effect of each parameter in the Højstrup model, a parametric study was conducted with z_i = 1000 m, and L = -100 m used as a benchmark. A reference mean wind speed U = 11.4 ms^{-1} was set at the height z = 90 m (these values were selected as they represent the rated wind speed and hub height of wind turbine used in this study). Table 1 summarises the parametric study and the simulated results of the u wind component turbulence intensity (TI). It can be seen from Table 1 that variations in z_i and L resulted in TI_u in the range of 5% to 9% and 6% to 9% respectively.

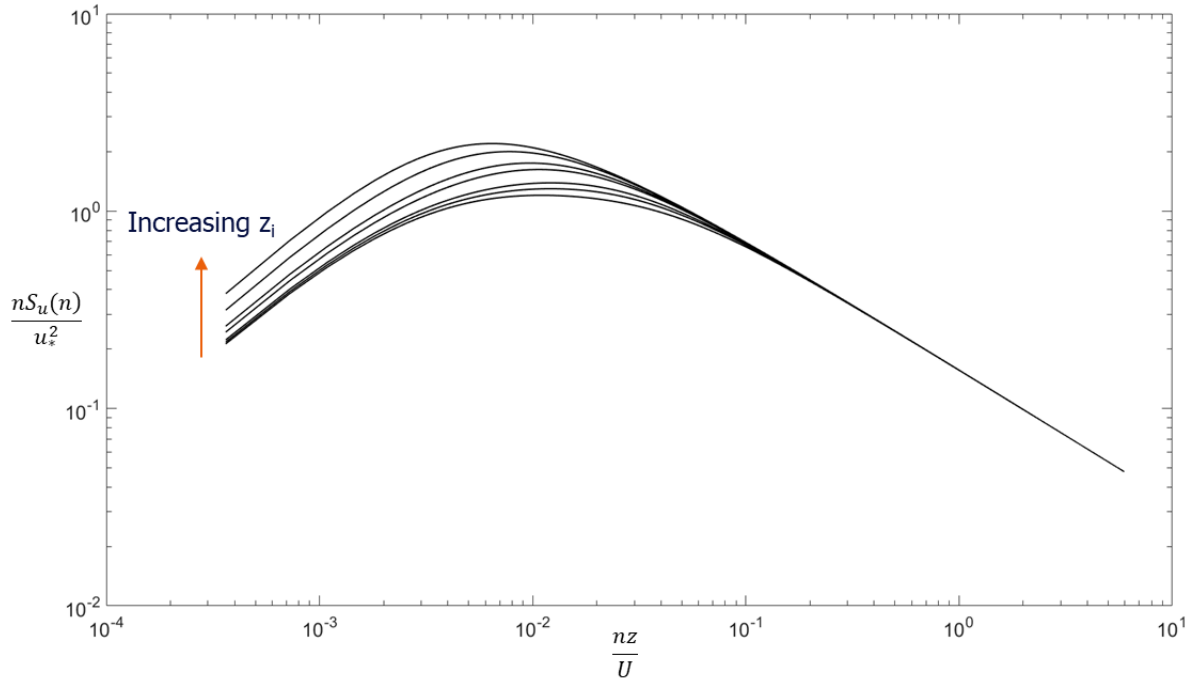

Figure 1. Spectra of u-component at z = 90 m for various z_i.

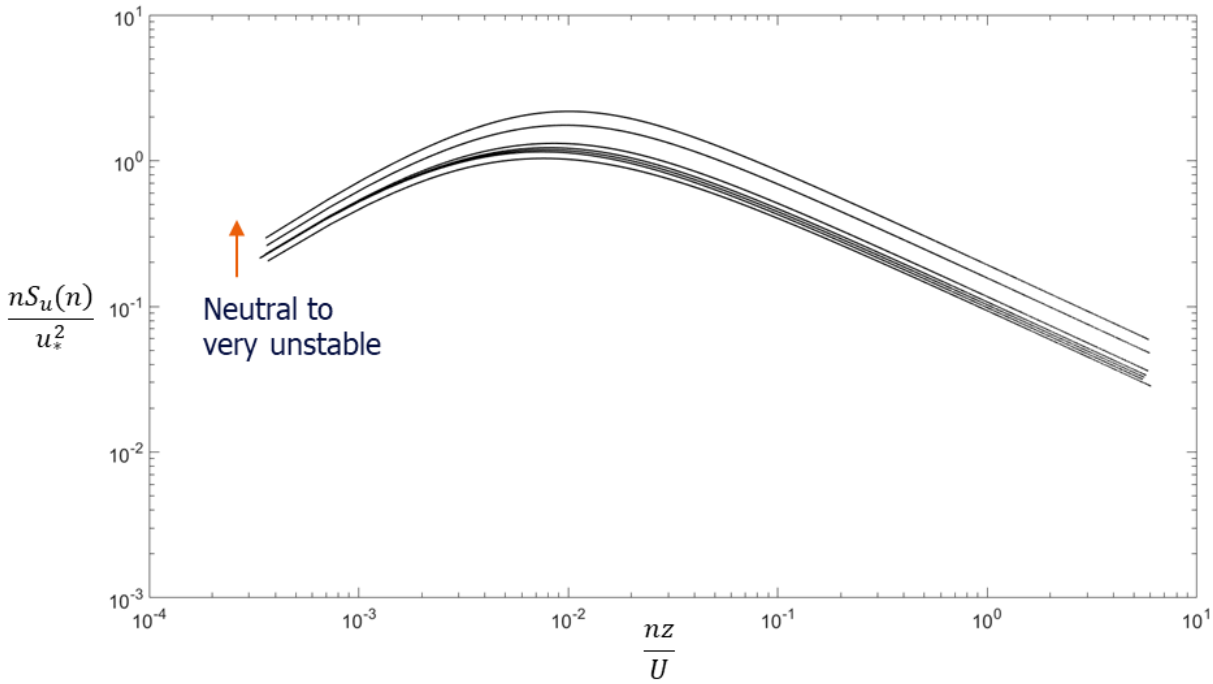

Figure 2. Spectra of u-component at z = 90 m for various L.

We observed that both inversion height z_i and Obukhov length L play an important role in the energy content of the Højstrup model. The increase in z_i on the Højstrup model resulted in increasing energy for u-wind components as presented in Figure 1, especially at low frequencies f (<0.05 Hz). At f>0.1Hz the influence of z_i diminishes and all converge to -2/3 line. This behaviour was also observed for v and w-components. The influence of z_i on the Højstrup model implies that higher z_i results in more energy only at lower frequencies.

Figure 2 shows the target spectra of the u-component comparing various L values at z = 90 m. As the stability goes from neutral to very unstable (from $L = \infty$ to L = -50 m), the u-spectra shifts up, indicating higher energy content as the atmospheric conditions becomes unstable. Unlike z_i, where its influence on the spectral content diminishes at higher frequencies, the higher energy content with variation in L was observed for all reduced frequencies.

3. Methodology

The simulations for this study were based on the spar-buoy type FOWT from Phase IV of the Offshore Code Comparison Collaboration (OC3) project [5]. This phase uses the 5 MW standard wind turbine of the National Renewable Energy Laboratory (NREL) with some changes in the support and control system, in conjunction with the spar-buoy concept 'Hywind' developed by Equinor [5]. The OC3-Hywind properties are summarised in Table 2.

Table 2. OC3-Hywind specifications.

Parameter	
Rotor configuration	3 bladed
Rotor diameter	126 m
Hub height	90 m (above sea level)
Cut-in, rated, cut-out wind speed	3, 11.4, 25 ms^{-1}
Cut-in, rated rotor speed	6.9 rpm, 12.1 rpm
Water depth	320 m
Draft	120 m
Mooring line	3 lines, 120^o apart from each other

3.1. Turbulent wind field simulations

Turbulent wind fields are required for structural simulations input and thus were generated prior to the simulations. The turbulent wind field is represented as a turbulence box with the size of 32768 x 32 x 32 nodes, respectively for along wind, cross wind, and vertical wind direction. A MATLAB model developed by Cheynet [8] was used to simulate the turbulent wind field. The number of nodes in the along wind direction represents the number of steps in the wind simulation. The Højstrup spectra S_u, S_v, and S_w were determined at each turbulence box node and Davenport coherence was used to compute the coherence at each frequency step. Similarly, the Kaimal spectra S_u, S_v, and S_w were determined at each turbulence box node along with Davenport coherence for coherence computation at each frequency step. The decay coefficients used in the Davenport coherence are given in Table 3 and were used for all load cases. According to the study by Cheynet et. al [13] who studied measured offshore wind data from the FINO 1 platform, these decay coefficients vary with stability conditions such that the co-coherence increases with progressively more unstable conditions. Therefore, the use of constant decay coefficients for different load cases given in Table 4 is an approximation, and thus is a limitation in this present study.

A random phase was then applied to the spectra at each node and each frequency step and finally Inverse Fast Fourier Transform (IFFT) was used to get the fluctuating wind speeds. The corrected

logarithmic wind profile from the DNV standards [14] was selected to represent the mean wind profile in our simulations. Accounting for the influence of atmospheric stability conditions, the mean wind velocity at a particular height is defined as [14]:

$$U(z) = \frac{u_*}{\kappa}\left[\ln\left(\frac{z}{z_0}\right) - \psi\right] \tag{9}$$

where κ is a constant (0.4) and ψ depends on the value of L, where for unstable conditions $L < 0$ [14]:

$$\psi = 2\ln(1+x) + \ln(1+x^2) - 2\,\mathrm{atan}(x) \tag{10}$$

in which $x = (1 - 19.3z/L)^{1/4}$. For neutral conditions ($L = \infty$), $\psi = 0$ and this was used for Kaimal model.

Six different random seeds were used for each load case to allow for the simulations to closely resemble the stochastic nature of wind and to reduce uncertainty in the simulations. The sampling frequency used in the simulations was approximately 9.1 s, corresponding to 3600 s simulations with the aforementioned time steps. A value of surface roughness of z_0 of 0.00014 m, was used based on measurements from [15] at the Høvsøre site, and u_{*0} of 0.4 ms^{-1} were used and kept constant in the simulations. The mean wind profile is computed by setting reference wind speed at the hub height U_{hub}. By utilising Eq. 9, the wind speed at height z relative to the hub height z_{hub} is calculated as:

$$U(z) = \frac{\left[\ln\left(\frac{z}{z_0}\right) - \psi\right]}{\left[\ln\left(\frac{z_{hub}}{z_0}\right) - \psi_{hub}\right]} U_{hub} \tag{11}$$

The load cases performed in this study are given in Table 4. Each load case was run for three different mean wind speeds: 8, 11.4, and 15 ms^{-1}, corresponding to below rated, rated, and above rated wind speed respectively.

Table 3. Decay coefficient used for Davenport Coherence Model.

Coefficient	C_u^y	C_v^y	C_w^y	C_u^z	C_v^z	C_w^z
Value	7	7	6.5	10	10	3

Table 4. Load cases.

Spectral model	z_i (m)	L (m)	Stability condition
Højstrup	700	-50	Very unstable
		-90	Unstable
		-180	Slightly unstable
	1000	-50	Very unstable
		-90	Unstable
		-180	Slightly unstable
Kaimal	700	∞	Neutral
	1000	∞	Neutral

3.2. Coupled SIMO-RIFLEX

SIMO-RIFLEX is a coupled simulation tool available in the Simulation Workbench for Marine Application (SIMA), which was developed by MARINTEK. SIMO is able to model flexible multibody systems and perform non-linear time domain simulation of surface vessels subjected to combined wind, wave, and current forces [16]. RIFLEX is a tool especially designed for analysis of slender marine structures with a finite element method that is able to handle unlimited displacements and rotations [10].

Within RIFLEX, there is an extension to include aerodynamic forces on elastic structural members (i.e. blades) using Blade Element Momentum (BEM) theory and control systems for blade pitch and electrical torque [10]. The coupled tools were necessary since the OC3-Hywind is a multibody surface vessel with slender elements.

The generated turbulent wind fields are stored in binary format and used as an input to the coupled SIMO-RIFLEX simulations. In addition to the wind loads described in subsection 3.1, wave loads were also included in our simulations. For all load cases given in Table 4, JONSWAP irregular waves with a peak parameter γ = 3.3, significant wave height H_S = 6 m, and peak period T_p = 12 s were defined. The SIMO-RIFLEX simulations used a 3600 s duration for each load case and each seed, with 0.02 s time step.

4. Results and discussion

In order to understand the simulation results better, results are presented under three different subsections: the simulated wind field characteristics, the fatigue loads of OC3-Hywind components, as well as the motion responses.

4.1. Simulated turbulent wind field

From section 2 we note that theoretically in the Højstrup model, parameters L and z_i affect both spectral energy and TI in a way that when the atmosphere becomes progressively more unstable, spectral energy and TI are increasing. A theoretical comparison between the Højstrup and Kaimal model shows that the Kaimal model has lower spectral energy (Figure 2) and TI (Table 1) than Højstrup model. This implies that neutral conditions produce lower levels of turbulence than unstable conditions. Figure 3 presents the TI from the turbulence box at height z = 92.5 m, and compares all load cases at different wind speeds. The turbulence box follows a sampling frequency of 9.1 Hz for a 1-hour average. The TI shown in Figure 3 are averaged from the six seeds for each case.

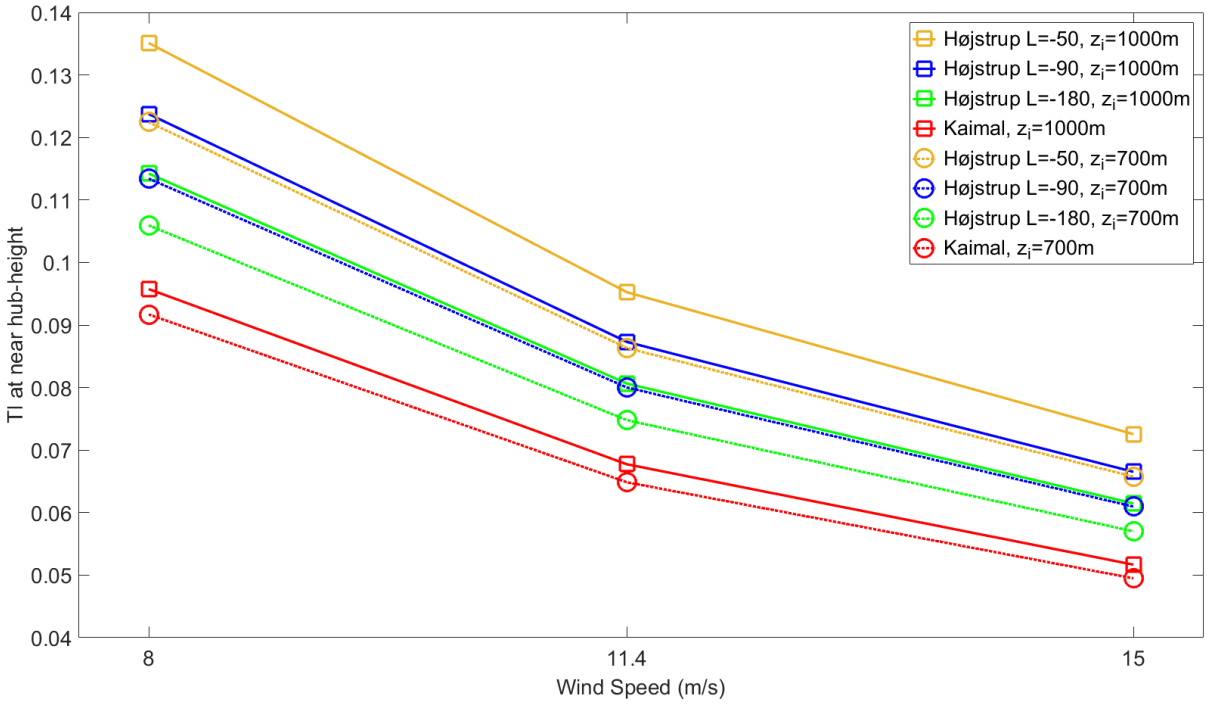

Figure 3. TI at z = 92.5 m from the simulations. Solid line for z_i = 1000 m, dotted line for z_i = 700 m.

In general, it is observed that TI is decreasing with increasing wind speed (Figure 3). We also noted that TI was decreasing with height. As shown in Figure 3, Højstrup with L = -50 m generated the highest TI followed by Højstrup with L = -90 m, L = -180 m and Kaimal respectively by considering the same z_i.

Comparing different z_i, it is clear that higher z_i results in higher TI, even though the effect of z_i on TI is not as pronounced as the effect of L (Figure 3). Variation in z_i gives approximately 14% difference between the maximum and minimum TI, while variation in L gives 40% difference between the maximum and minimum TI (Figure 3). This effect of z_i was also noted for the Kaimal model despite z_i not being an input parameter in the model (Figure 3) but is included via the u_* value in Eq. 8 which incorporates z_i.

4.2. Damage equivalent loads

Fatigue loads of the OC3-Hywind turbine components are measured in the form of damage equivalent load (DEL). Rainflow counting method [17] was used as the stress range filter. To quantify the DEL from load time series, the relation between the occurring stress and its number of cycle is required. This relation is commonly known as S-N curve and is usually obtained by experiments for different materials. In the absence of a S-N curve, the number of cycles N_i resulting in failure at a specific stress S_i can be determined with $N_i = S_0^m S_i^{-m}$, where S_0 is the highest stress in the time series and m is the Wöhler exponent. Normally, a quantified equivalent damage S_{eq} for a given number of cycles n_{eq} is considered to make an easier interpretation of the accumulated loads $D_{total} = n_{eq}\, S_{eq}^m$. By substituting $D_{total} = \sum n_i S_i^m$, the damage equivalent load is calculated as [18]:

$$S_{eq} = \left(\frac{\sum n_i S_i^m}{n_{eq}} \right)^{1/m} \tag{12}$$

where n_i is the number of cycle occurrences for the considered load range class, obtained from rainflow counting along with S_i. In the calculation, the value of n_{eq} = 10^7, m = 3 for tower and mooring line components (steel material), and m = 12 for blade (fiberglass material) were selected. DEL of the OC3-Hywind turbine were computed for the following wind turbine load components: tower base fore-aft bending, tower base side-side bending, tower top torsion, blade root flap-wise bending, blade root edge-wise bending, and mooring lines tension. DEL results are presented in the normalised form relative to the load case of Kaimal z_i = 1000 at 8 ms^{-1}. The normalised DEL shown in Figure 4 to Figure 6 are the averaged values from all six seeds.

We note that in general, the Højstrup model with L = -50 m resulted in the highest DEL followed by Højstrup with L = -90 m, L = -180 m and finally Kaimal by comparing the same z_i. This was observed for each of the aforementioned load components, except for the mooring lines tension where no clear pattern was seen. Below rated wind speed (8 ms^{-1}) very unstable conditions (L = -50 m) resulted in higher DEL for both values of z_i. At rated wind speed and above (11.4 ms^{-1} and 15 ms^{-1}), exceptions were noted for the tower base fore-aft bending and the blade root flap-wise DEL's (Figure 6), which showed no obvious trends. When comparing different z_i, generally higher z_i resulted in higher DEL's with the Kaimal model and z_i = 700 giving the lowest DEL's, compared to other load cases.

As presented in Figure 4, the largest DEL variation between load cases was observed for the tower top torsion with 65% difference between the minimum and the maximum values. The second largest DEL variation with 37% difference between the minimum and the maximum values was observed for the tower base side-side bending as shown in Figure 5. On the other hand, the least DEL's variation was noted for blade root edge-wise bending with only 3% difference between the minimum and the maximum values. A small DEL's variation of 7% was also observed for the tower base fore-aft. Mooring line 3 tension DEL's varied by 25% when comparing minimum and the maximum values, which is the highest variation amongst the three lines. Our simulations also resulted in a 24% difference between the minimum and the maximum values for the blade root flap-wise bending DEL's.

In respect to variation in wind speed, normally the DEL increases with wind speed as shown in Figure 4 for the tower top torsion DEL's. The increase of the DEL with wind speed was also observed for other load components, except for tower base side-side bending DEL's which seemed to decrease with wind speed (Figure 5). Meanwhile, mooring lines tension DEL's showed no specific pattern with wind speed.

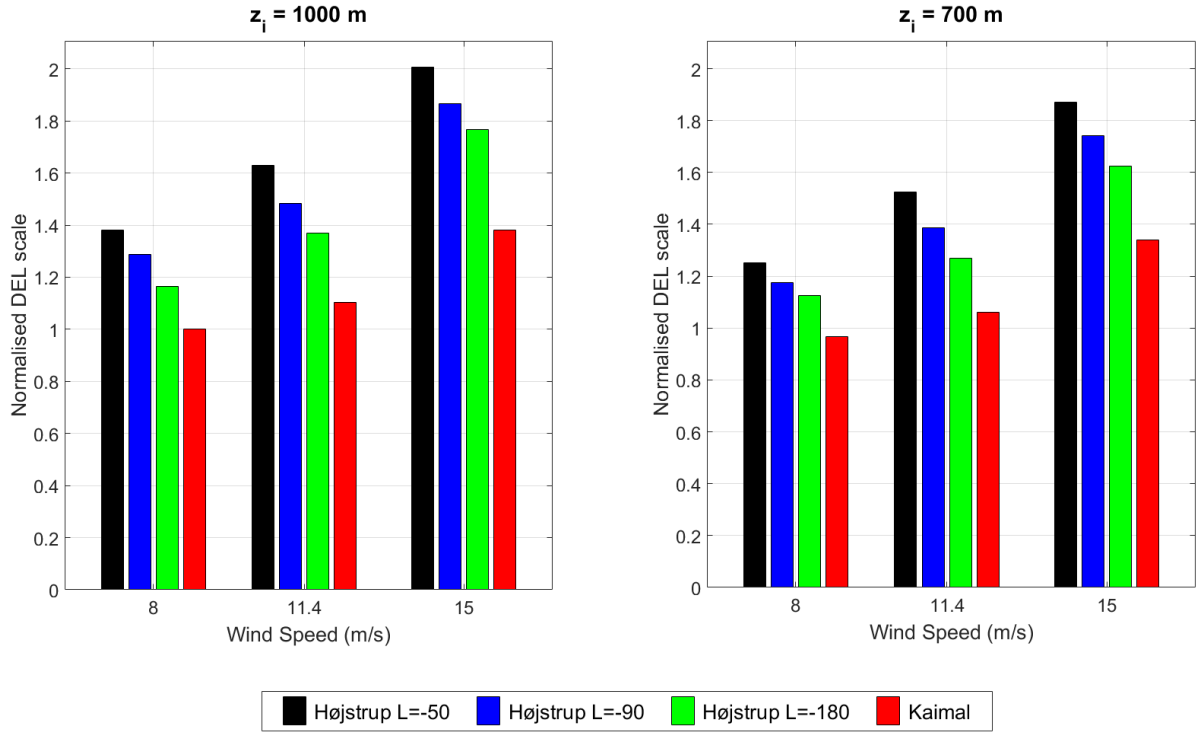

Figure 4. Normalised DEL for tower top torsion (normalized by the load case of Kaimal at 8 ms^{-1}). Left figure shows the results for z_i = 1000 m and the right hand figure for z_i = 700 m.

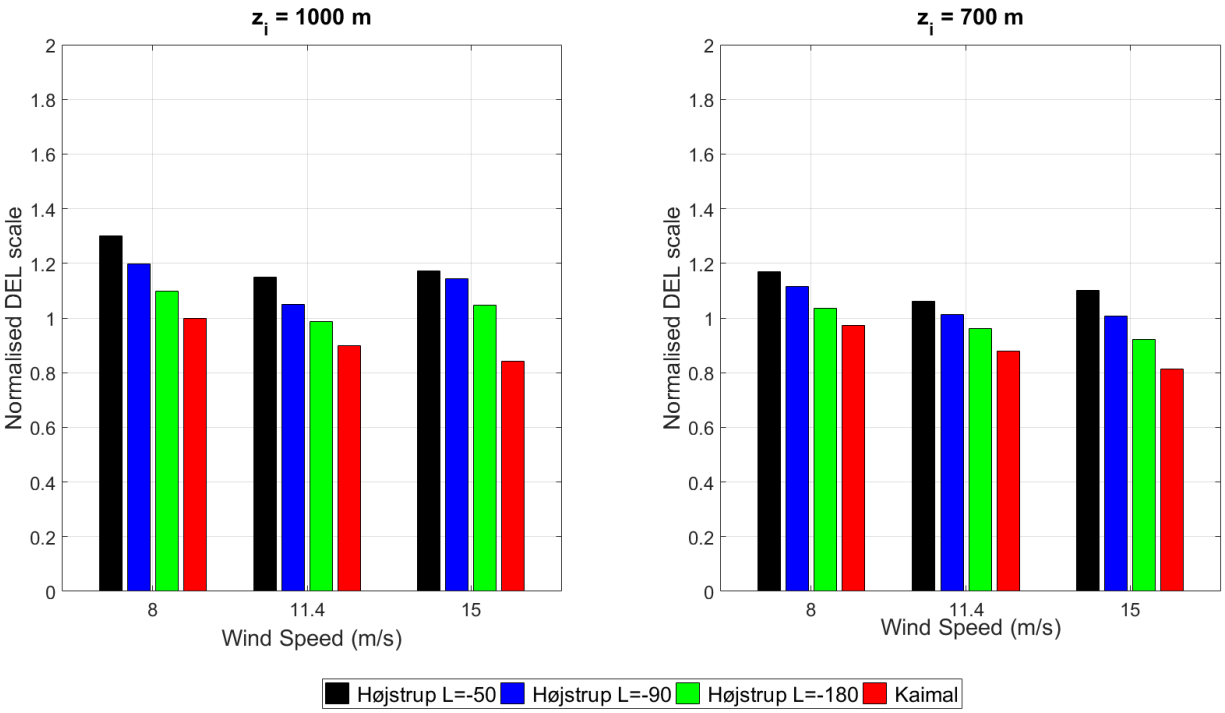

Figure 5. Normalised DEL for tower base side-side bending (normalized by the load case of Kaimal at 8 ms^{-1}). Left figure shows the results for z_i = 1000 m and the right hand figure for z_i = 700 m.

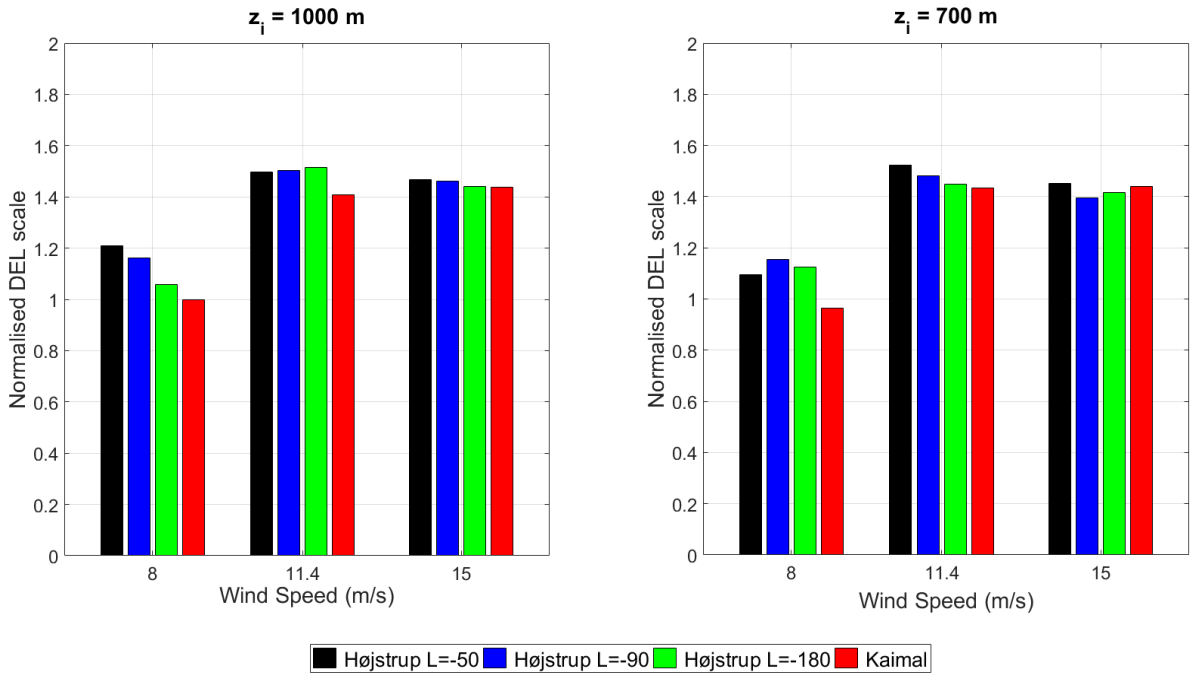

Figure 6. Normalised DEL for blade root flap-wise bending (normalized by the load case of Kaimal at 8 ms^{-1}). Left figure shows the results for z_i = 1000 m and the right hand figure for z_i = 700 m.

Figure 7 shows the spectral density plot of tower top torsion comparing neutral to very unstable stability conditions for U = 11.4 ms^{-1} and z_i = 1000 m. It can be seen that the highest spectral energy is found for Højstrup with L = -50 m, followed by Højstrup L = -90 m, Højstrup L = -180 m, and Kaimal, observed for all frequencies except at 0.2 Hz. The tower top torsion is excited by waves at frequency f = 0.083Hz, blade 1P (f = 0.2 Hz) and blade 3P (f = 0.6 Hz). The same was observed for all other wind speeds. When comparing the same results for z_i = 1000 m and z_i = 700 m, in general a similar trend was observed except at f = 0.2 Hz where Højstrup with L = -50 m produced the highest spectral energy. The boundary layer height of z_i = 700 m was also observed to result in lower energy spectra when compared to the results for z_i = 1000 m for all Højstrup cases.

The spectral energy density plots for the tower base side-side bending also showed that the highest spectral energy was found under very unstable conditions (Højstrup with L = -50 m) similar to the tower top torsion. Particularly at frequencies f < 0.15 Hz and f > 0.45 Hz whereas at 0.15 Hz < f < 0.45 Hz, the variation between the load cases was quite small. The highest spectral peak is found for f ~ 0.5 Hz which corresponds to the tower base side-side bending natural frequency. Similarly, this trend was observed for other wind speeds except that at 8 ms^{-1}, where the magnitude of the spectral energy is notably higher particularly near the natural frequency of the tower base side-side mode. Comparing z_i=1000 m and z_i= 700 m, in general a similar trend was observed and lower z_i was observed to result in lower energy spectra for all Højstrup cases.

The spectral energy of the blade root flap-wise bending shows that this mode was excited by the wave frequencies, blade 1P, 2P, and 3P at all considered wind speeds. At frequencies lower than 1P, the spectral energy showed no notable variation with different stability conditions. At frequencies higher than 1P, one can note that generally Højstrup with L = -50 m resulted in the highest spectral energy followed by Højstrup L = -90 m, Højstrup L = -180 m, and Kaimal. However, in the peak of 1P, 2P, and 3P spectral energy of Kaimal case overlapped with Højstrup with L = -50 m especially at rated wind speed and above. A similar trend was noted for the z_i = 700 m, except it produced lower energy spectra than when z_i = 1000 m for all Højstrup load cases.

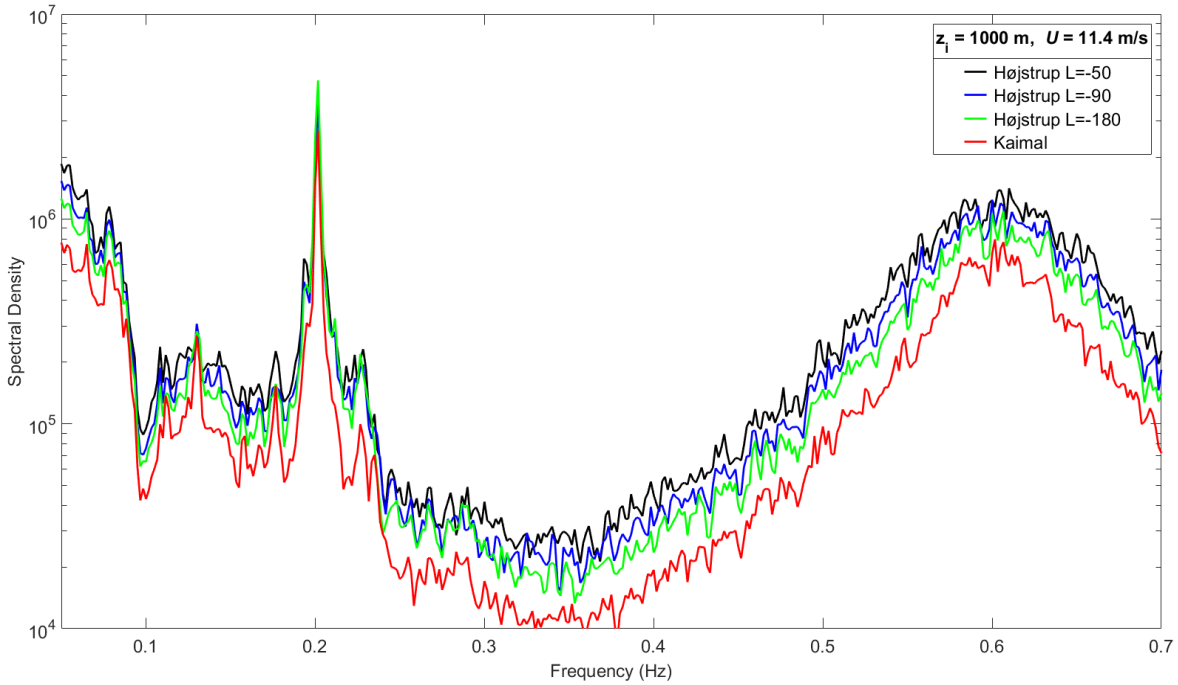

Figure 7. Spectral density plot of tower top torsion for U = 11.4 ms^{-1} at z_i = 1000 m.

4.3. Platform motions

Aside from fatigue damage (DEL's), it is also important to evaluate the motions in six DOF experienced by the OC3-Hywind. Our simulations showed that the roll, sway and yaw platform motions exhibited notable differences between the load cases as opposed to pitch, surge and heave. In this subsection, emphasis is put on platform roll and sway, however, it is important to note that the magnitude of both sway translation and roll motion were very small, within the range of -1 m to 1 m for sway and -0.3^o to 0.6^o for roll.

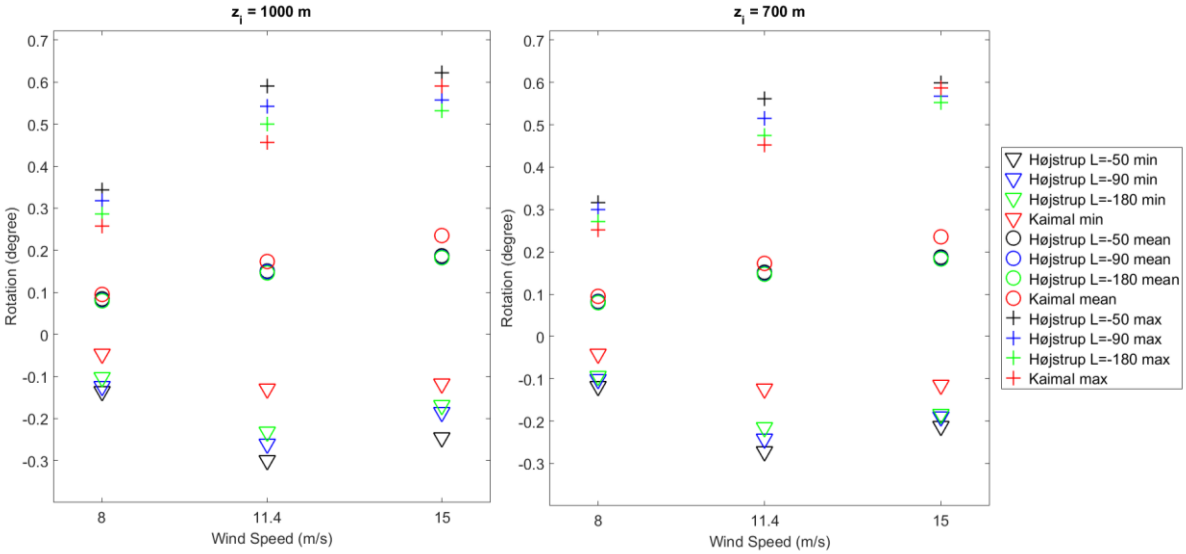

Figure 8. Platform roll rotation (all load case). Left figure z_i = 1000 m, right figure for z_i = 700 m.

Figure 8 presents platform roll of the OC3-Hywind comparing all load cases. It can be seen from this figure that generally Højstrup with L = -50 m resulted in the highest roll followed by Højstrup L=-90 m, L= -180 m and finally Kaimal. Comparing the left and right plots in Figure 8, the influence of z_i on platform roll motion was not notable since the overall platform roll distribution is relatively similar for both boundary layer heights.

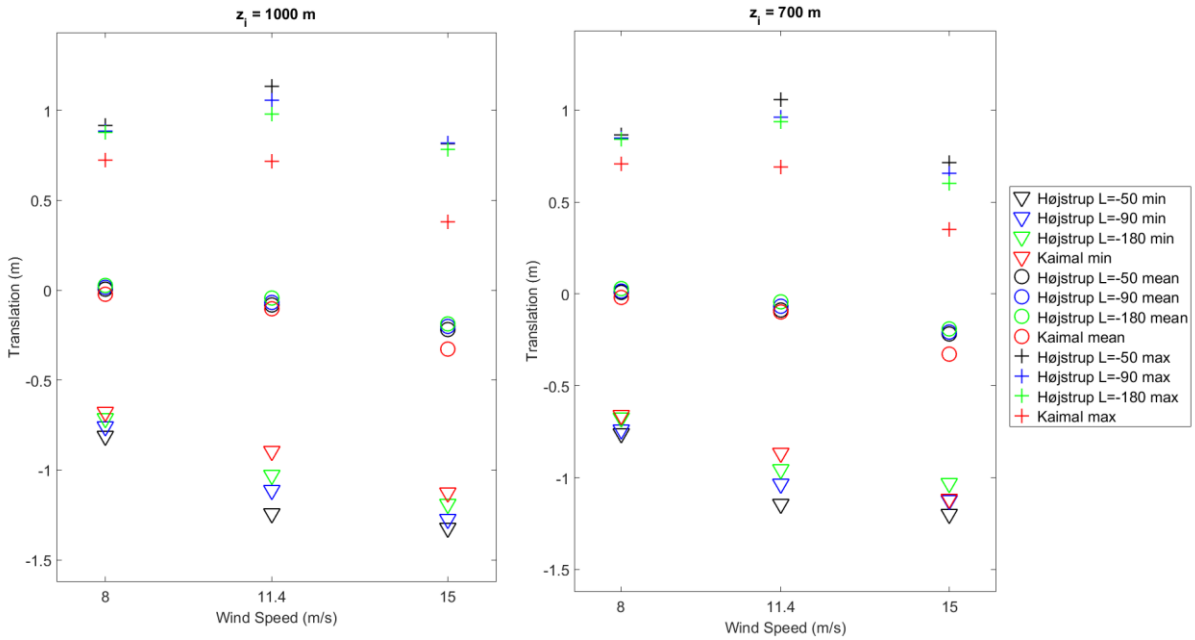

Figure 9. Platform sway translation (all load case). Left figure z_i= 1000 m, right figure for z_i= 700 m.

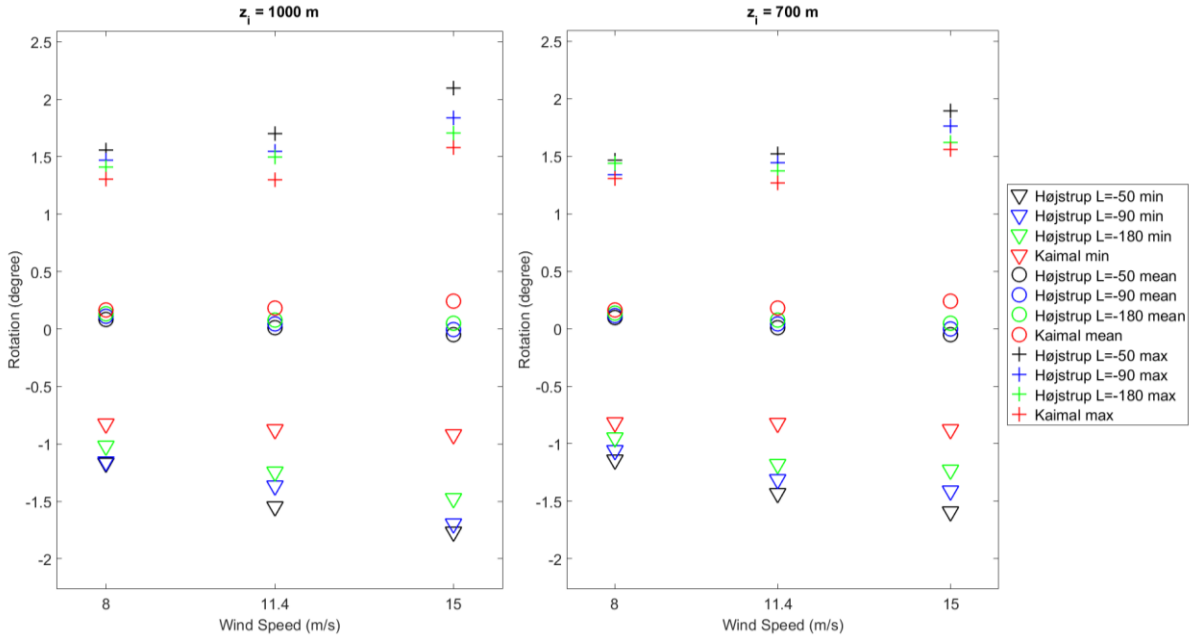

Figure 10. Platform yaw rotation (all load case). Left figure z_i = 1000 m, right figure for z_i = 700 m.

The platform sway response comparing all load cases is shown in Figure 9. As seen from this figure, one can observe a similar trend with the platform roll response where generally the highest sway was

found under Højstrup with L = -50 m, followed by Højstrup with L = -90 m, L = -180 m and Kaimal respectively. Likewise for roll motion, the influence of z_i on platform sway was not notable.

Platform yaw response comparing all load cases can be seen in Figure 10. This figure shows that Højstrup with L= -50 m generally yielded the highest platform yaw followed by Højstrup L = -90 m, L = -180 m and finally Kaimal. The effect of z_i on platform yaw was also not clearly observed.
In terms of spectral energy, platform roll, sway, and yaw motions were excited by the waves and generally, Højstrup with L = -50 m gave the highest spectral energy for roll, sway, and yaw followed by Højstrup with L = -90 m, L = -180 m and Kaimal. The highest spectral peak for platform roll was noted at the platform's roll natural frequency f ~ 0.034 Hz for all load cases. The same was observed for sway where the platform's sway natural frequency at f ~ 0.0073 Hz had the highest spectral peak for all load cases. For yaw motion, the highest spectral peak was found at low frequency f ~ 0.005 Hz, which might be the excitation from the low frequency content in the Højstrup spectral wind model for all unstable load cases. Comparing z_i = 1000 m and z_i = 700 m, higher z_i generally resulted in higher spectral energy for platform roll, sway, and yaw.

4.4. Discussion

The parameters L and z_i seem to affect the generated TI, where TI is increasing with z_i and with L as z/L<0 gets closer to zero. This is in agreement with the sensitivity study performed in section 2. The influence of the parameters L and z_i on the generated TI can also be related to the DEL's and platform motion responses, such that higher TI results in higher DEL's and platform motion, when considering the same wind speed.

When comparing the Højstrup and Kaimal wind models, one can see that the addition of lower spectral frequency components to represent unstable atmospheric conditions has resulted in higher energy spectra for u, v, and w wind components. This addition also produces higher TI as well as DEL's and platform motions of the OC3-Hywind turbine. Based on this argument, we are able to simulate the effect of enhanced turbulence levels under unstable atmospheric stability unlike previous studies which have used for example the Mann spectral tensor model fitted to measurements under unstable atmospheric conditions [16]. Having said the above, exclusions were applicable to the following components:

- Mooring lines tension DEL has no clear trends for progressively unstable conditions or even increasing wind speed
- Despite the finding that platform pitch motion did not vary much with load case variation, it is worth mentioning that the OC3-Hywind platform was found to be dominated by pitching backwards (the platform pitched in the range of -2^o to +8^o). This platform pitch response might be due to the influence of the blade-pitching activity [19]
- Platform pitch, heave, and surge motions seemed to be 'invariant' with load case variation for the OC3 Hywind turbine, probably due to these DOF being heavily influenced by the wave excitation. We noted that the spectral plots of these DOF were very similar for all load cases, especially near the peak wave frequency.

Lastly, although z_i is not an input parameter to Kaimal Model, the influence of z_i on the generated TI and DEL is probably due to the use of an approximated u_*value, given in equation 8, which involves z_i.

5. Conclusion

From this study, the importance of unstable atmospheric stability on the loads and motion responses of the OC3-Hywind turbine is highlighted. By using the Højstrup model to account for enhanced energy at low frequencies under unstable conditions, the DEL of tower top torsion is estimated to be 65% higher than in neutral conditions using the Kaimal model, similarly for the tower base side-side bending DEL which was 37% higher. It was also found that the use of an appropriate wind model for unstable

conditions can produce up to 40% higher TI compared to neutral conditions. It is therefore necessary to account for unstable conditions in the design of FOWTs, as unstable conditions are prominent in an offshore environment [4] [13]. It is therefore important to develop and validate a turbulent wind model suitable for unstable conditions in the offshore marine boundary layer, to reduce the uncertainty in the design of large floating offshore wind turbines.

Acknowledgments
Authors would like to express their gratitude to Dr. Etienne Cheynet, for the assistance, knowledge, support, and time spent to help in the completion of this article.

References

[1] C. Dyrbye and S. O. Hansen, Wind Loads in Structure, West Sussex, England: John Wiley & Sons Ltd, 1997.

[2] International Electrotechnical Commission, "Wind Turbines – Part 1 Design Requirements," International Electrotechnical Commission (IEC), Geneva, Switzerland, 2005.

[3] J. Mann, "The Spatial Structure of Neutral Atmospheric Surface-layer Turbulence," *Journal of Fluid Mechanics 273,* pp. 141 - 168, 1994.

[4] O. Krogsæter and J. Reuder, "Validation of Boundary Layer Parameterization Schemes in the Weather Research and Forecasting (WRF) Model under the Aspect of Offshore Wind Energy Applications-Part II: Boundary Layer Height and Atmospheric Stability," *Wind Energy 18(7),* pp. 1291 - 1302, 2014.

[5] J. Jonkman, "Definition of the Floating System for Phase IV of OC3," National Renewable Energy Laboratory (NREL), Golden, CO, USA, 2010.

[6] J. Højstrup, "A Simple Model for the Adjustment of Velocity Spectra in Unstable Conditions Downstream of an Abrupt Change in Roughness and Heat Flux," *Boundary-Layer Meteorology 21,* pp. 341 - 356, 1981.

[7] J. C. Kaimal, J. C. Wyngaard, Y. Izumi and O. R. Coté, "Spectral Characteristics of Surface-layer Turbulence," *Quarterly Journal of the Royal Meteorological Society, 98(417),* pp. 563 - 589, 1972.

[8] E. Cheynet, "Wind Field Simulation," MathWorks, 2018.

[9] A. G. Davenport, "The Spectrum of Horizontal Gustiness Near the Ground in High Winds," *Quarterly Journal of the Royal Meteorological Society 83(372),* pp. 194 - 211, 1961.

[10] H. Ormberg and E. Bachynski, "Global Analysis of Floating Wind Turbines: Code Development, Model Sensitivity and Benchmark Study," *Twenty-second International Offshore and Ploar Engineering Conference,* 17-22 June 2012.

[11] J. Højstrup, "Velocity Spectra in the Unstable Planetary Boundary Layer," *Journal of the Atmospheric Sciences 39(10), ,* pp. 2239 - 2248, 1982.

[12] A. Monin and A. Obukhov, "Basic Laws of Turbulent Mixing in the Surface Layer of the Atmosphere," *Contrib. Geophys. Inst. Acad. Sci. 24(151),* pp. 163 - 187, 1954.

[13] E. Cheynet, J. B. Jakobsen and J. Reuder, "Velocity Spectra and Coherence Estimates in the Marine Atmospheric Boundary Layer," *Boundary-Layer Meteorology 169(3),* pp. 429 - 460, 2018.

[14] Det Norske Veritas AS, "Environmental Conditions and Environmental Loads (DNV-RP-C205)," Oslo, 2014.

[15] A. Sathe, J. Mann, T. Barlas, W. A. A. M. Bierbooms and G. J. W. van Bussel, "Influence of Atmospheric Stability on Wind Turbine Loads," *Wind Energy 16(7),* pp. 1013 - 1032, 2013.

[16] MARINTEK, 2009. [Online]. Available: http://www.ivt.ntnu.no/imt/courses/tmr4225/lectures/2009/Lecture%20Notes_Finn%20G%20Nielsen/2009-03-17_Simo%20and%20Mathiue/SIMO_general_PCS.pdf. [Accessed December 2018].

[17] M. Matsuishi and T. Endo, "Fatigue of Metals Subjected to Varying Stress," *Japan Society of Mechanical Engineers, Fukuoka, Japan, 68(2),* pp. 37-40, 1968.

[18] DTU Wind Energy, "DTU Itslearning," [Online]. Available: https://windenergy.itslearning.com/ContentArea/ContentArea.aspx?LocationID=29&LocationType=1. [Accessed 2016].

[19] M. Hall, B. Buckham and C. Crawfor, "Evaluating the Importance of Mooring Line Model Fidelity in Floating Offshore Wind Turbine Simulations," *Wind Energy 17(12),* pp. 1835 - 1853, 2014.

[20] A. Sathe, S. E. Gryning and A. Peña, "Comparison of the Atmospheric Stability and Wind Profiles at Two Wind Farm Sites Over a Long Marine Fetch in the North Sea," *Wind Energy 14(6),* pp. 767-780, 2011.